Ocean Dynamics (2016) 66:1317–1332
DOI 10.1007/s10236-016-0991-6

The eddy-dipole mode interaction and the decadal variability of the Kuroshio Extension system

Dehai Luo[1] · **Shaohua Feng**[2] · **Lixin Wu**[2]

Received: 22 March 2016 / Accepted: 5 September 2016 / Published online: 14 September 2016

Abstract In this paper, the physical cause of why the eddy kinetic energy (EKE) in the upstream Kuroshio Extension (KE) region is strong (weak) during a large (small) jet meandering period is studied by using the satellite altimeter data and constructing an eddy-dipole mode interaction theory from a reduced gravity shallow water wave quasi-geostrophic vorticity equation. It is found that the large KE jet meander corresponds to a large-scale positive-over-negative dipole SSH anomaly (KED^- mode, hereafter), a double-branch jet with a weak strength and a strong EKE in the upstream KE region, while the small jet meander corresponds to a negative-over-positive dipole anomaly (KED^+ mode, hereafter), a strong single-branch jet, and a weak EKE. Further diagnostics using this new eddy-dipole mode interaction theory reveals that the horizontal advection and KED deformation field can change the eddy activity in the upstream KE region. When the KED^- mode is amplified by mesoscale eddies, the EKE grows by extracting energy from the KED^- deformation (shearing and stretching) field and due to a reduced eastward advection, thus showing a high EKE level during the KED^- mode (large jet meander) episode. In contrast, when the KED^+ mode is intensified, the kinetic energy of the eddy weakens by losing its energy to the KED^+ deformation field and by an enhanced eastward advection, thus showing a low EKE level during the KED^+ mode (small jet meander) episode. Because the KED mode shows a clear decadal variation due to the modulation of the Pacific Decadal Oscillation, both the KE jet and EKE exhibit inevitably a distinct decadal variability.

Keywords Kuroshio Extension · Dipole mode · Eddies · Eddy-dipole mode interaction · Decadal variability

Responsible Editor: Leo Oey

✉ Dehai Luo
ldh@mail.iap.ac.cn

[1] RCE-TEA, Institute of Atmospheric Physics, Chinese Academy of Science, Beijing 100029, China

[2] Qingdao Collaborative Innovation Center of Marine Science and Technology and Physical Oceanography Laboratory, Ocean University of China, Qingdao, China

1 Introduction

The western boundary current in the North Pacific Ocean is separated from the coast of Japan near 140 ° E and 35 ° N and then forms a Kuroshio Extension (KE) system as an inertial extension. The striking feature of this system is that there is a clear decadal transition between large and small amplitude meander states with high and low eddy kinetic energy (EKE) levels (Kawai, 1972; Wyrtki 1975; Mizuno and White 1983; Deser et al. 1999). Because intense sea-air heat exchange and water mass exchange take place over the KE region, the air-sea interaction in midlatitudes and North American climate on interannual and decadal timescales are likely related to the variation of the KE system (Latif and Barnett 1994; Liu and Wu 2004). In past decades, the variability of the KE system and its dynamics has been an important topic (Jiang et al. 1995; McCalpin and Haidvogel 1996; Seager et al. 2001; Nonaka et al. 2006; Pierini 2006; Berloff et al. 2007a, b; Taguchi et al. 2007; Pierini et al. 2009; Waterman et al. 2011; Sasaki et al. 2013).

The analysis using the satellite altimeter data reveals that the KE system such as the KE jet meandering and EKE exhibit a clear decadal variability (Seager et al. 2001; Qiu and Chen 2005, 2010; Pierini 2006, 2014). Many studies have suggested that the decadal variability of the KE system is not only related

to westward propagating signals from the central and eastern North Pacific (Ceballos et al. 2009; Sasaki et al. 2013) but also related to a decadal self-sustained oscillation or turbulent (eddy-driven) oscillator (Pierini 2006; Berloff et al. 2007a). Pierini (2006) used a reduced gravity shallow water model to indicate that under a time-independent wind stress forcing, the KE system can exhibit a decadal chaotic bimodal self-sustained oscillation between an energetic meandering state and a much weaker state with a reduced penetrating jet, thus indicating that the nonlinear dynamics in the KE region is important for the KE decadal variability. The study of Berloff et al. (2007a) also indicated that the KE system resembles a decadal turbulent oscillator driven by the mesoscale eddies via the eddy-mean flow interaction. This hints that the variability of the KE system is a complicated nonlinear phenomenon of the eddy-mean flow interaction. Because a time-average is used in the derivation of the previous eddy-mean flow interaction model and because the eddy equation vanishes (Hoskins et al. 1983), it is difficult to use this kind of the eddy-mean flow interaction theory to explain the variation of the EKE in the upstream KE region during the large (small) meandering period of the KE jet. This motivates us to develop a new eddy-dipole mode interaction theory to explore the physical cause of the decadal variation of the KE system. On this basis, we present a new viewpoint that the horizontal deformation of the large-scale dipole (KED) mode in the upstream KE region is important for the decadal variability of the KE system through decadal changes in the phase and frequency of KED events. Moreover, an observational analysis from the satellite altimeter data is presented to support this viewpoint.

Because our focus is placed on the variation of the sea-surface height anomaly in the upstream KE region, in this paper, it is reasonable to use the reduced gravity shallow water wave (RGSW) equations to construct an eddy-dipole mode interaction theory in the KE system similar to the recent work of Luo et al. (2015) under a quasi-geostrophic assumption. The use of the RGSW model is reasonable at least for the dynamical study of the KE variability even though the KE system is approximately equivalent barotropic. Actually, the RGSW equations have been widely used to investigate the dynamics of the KE variability (Jiang et al., 1995; Pierini 2006; Pierini et al. 2009; Sasaki et al. 2013).

This article is organized as follows: In Section 2, we describe data and method. In Section 3, a jet width index is defined to characterize the meander extent of the KE jet, and the main results are presented by proposing a large-scale dipole (KED) mode and defining its index based on the satellite altimeter data during 1993–2010. A new eddy-dipole mode interaction model as a description of the KE system is presented in Section 4. In particular, in this section, the dipole mode and eddy equations are derived, respectively, under the scale separation and quasi-geostrophic assumptions. The diagnostic results using this eddy-dipole mode interaction model are presented in Section 5 to demonstrate that the different deformation field of the KED mode in the upstream KE region is important for the variation of the EKE between strong and weak meandering states. The explanation for the physical cause of the EKE decadal variability is presented in Section 6. Conclusion and discussions are summarized in the final section.

2 Data and methodology

We use the daily satellite altimeter sea-surface height (SSH) data with the resolution of 0.25° × 0.25° from January 1993 to December 2010 (http://www.aviso.altimetry.fr/en/data.html). In this paper, the SSH field $h(x, y, t)$ is decomposed into the climatological mean $h(x, y)$, low-frequency (>300 days) $h_L(x, y, t)$ and high-frequency $h'(x, y, t)$ (≤300 days) anomaly fields. Here, we define high-frequency transient anomaly $h'(x, y, t)$ as the high-frequency or mesoscale eddies and the low-frequency SSH anomaly $h_L(x, y, t)$ with a dipole meridional structure as the large-scale KE dipole (KED, hereafter) mode.

To reflect the variability of the KE system, three indices are defined here. First, we define the mean value of $\delta h = -\frac{\partial h}{\partial y}$ greater than 0.2 averaged over the region (141° E–165° E, 32° N–38° N) as the KE jet strength (Qiu and Chen 2005) because the strength of the KE jet can be characterized by the zonal geostrophic velocity $u = -\frac{g}{f}\frac{\partial h}{\partial y}$ of the SSH field (where f is the Coriolis parameter and g is the gravity acceleration). Second, we calculate $(u'^2 + v'^2)/2$ in terms of $(u', v') = \left(-\frac{g}{f}\frac{\partial h'}{\partial y}, \frac{g}{f}\frac{\partial h'}{\partial x}\right)$ as the eddy kinetic energy (EKE). Then, the mean value of the EKE over an area covered by the values of EKE equal to or greater than 0.02 m^2/s^2 over the region (141° E–153° E, 32° N–38° N) is defined as the EKE intensity in the upstream KE region. Finally, a jet width index, $W = \frac{\sum_{i=1}^{n_x} n_{yi}}{n_x}$ is defined to describe the variability of the KE jet meander, where n_{yi} denotes the number of the meridional grid points at the zonal grid point i for the KE current velocity $u \geq u_c$ (u_c is a threshold), and n_x represents the number of the zonal grid point for $u \geq u_c$. In following discussions, we choose $u_c = 0.1$ m/s as a threshold of the KE current velocity.

Based on the magnitude of the W value, we can select the large or small meander events of the KE jet. This is undertaken below.

3 Results from the satellite altimeter data

3.1 Jet width index and jet meander

As noted above, the jet width index characterizes the meander extent of the KE jet. Thus, we can pick jet meander events by calculating the jet width index. In fact, the positive (negative) value of the normalized jet width index W corresponds essentially to a broadening (narrowing) of the KE jet. To further understand the relationship between the jet width and the jet meander, in this subsection, we use the yearly mean satellite altimeter data. We define a jet event with the yearly mean jet width index equal to or greater (less) than a +0.4 (−0.4) standard deviation as a weak wide jet or WWJ (strong narrow jet or SNJ) event. Of 18 events, there are six (1996, 1997, 1999, 2001, 2006, and 2007) WWJ and five (1994, 2002, 2003, 2004, and 2010) SNJ events. By performing an average of yearly mean SSH fields and zonal currents for all WWJ or SNJ events, it is feasible to understand whether the large jet meander corresponds to a wide jet.

We show the yearly mean SSH, zonal current, and EKE fields averaged for six WWJ and five SNJ events in Fig. 1. It is seen that the average SSH field exhibits a strong large-scale ridges north of about 35°N for WWJ events (Fig. 1a). For this case, the anticyclonic recirculation to the south of 35°N is relatively weak. Such a spatial structure reflects a large KE jet meander. However, for SNJ events, the average SSH field exhibits a strong anticyclonic (cyclonic) recirculation to the south (north) of 35°N (jet axis), thus reflecting that the KE jet is strong and is referred to as a small KE jet meander (Fig. 1b). Figure 1c, d is the corresponding zonal currents of the average SSH fields shown in Fig. 1a, b. We can see that in an average zonal current field, the KE jet is weak and split into two branches in the upstream region (141° E–153° E) of the KE for WWJ events (Fig. 1c), while it is strong and exhibits a single-branch jet structure for SNJ events (Fig. 1d). Also, it is easy to see that the meridional position of the jet core is distinctly different between WWJ and SNJ events. Figure 1e (Fig. 1f) further shows that the mean EKE is strong (weak) for WWJ (SNJ) events. Thus, the above result poses an important question of what determines the variations of the EKE and the jet meander state in the upstream KE region.

To clearly see the mutual relationship between the meandering of the KE jet and the EKE, it is useful to show the anomaly fields of the average SSH and zonal current in Fig. 2 for WWJ and SNJ events. A comparison with Fig. 1a, b shows that the large (small) jet meander corresponds to a positive-over-negative (negative-positive-positive) dipole height anomaly in the upstream KE region in Fig. 2a (Fig. 2b), which is referred to as the negative (positive) phase of the KED mode or a KED^- (KED^+) mode hereafter. In an average anomaly field, the zonal current shows a clearer double-branch jet structure in Fig. 2c for the KED^- mode, while a prominent single-branch jet structure is seen in Fig. 2d for the KED^+ mode. Thus, the presence of a double-branch or a single-branch jet structure reflects the weakening and widening or strengthening and narrowing of a KE jet in the total zonal current field as shown in Fig. 1c or in Fig. 1d. In this case, it is concluded that the KED^- mode (Fig. 2a) corresponds essentially to a double-branch jet with a weak strength (Fig. 1c or Fig. 2c) and a strong EKE level (Fig. 1e), while the KED^+ mode (Fig. 2b) has a strong single-branch jet (Fig. 1d or Fig. 2d) and a weak EKE level (Fig. 1f). According to the geostrophic balance, an intensified double- (single-) branch jet structure occurs inevitably when an intensified KED^- (KED^+) mode appears in the upstream KE region and vice versa. Thus, the changes in the KED phase and the spatial structure of the KE jet are a simultaneous phenomenon of their mutual adjustment. As noted below, because the KED can be amplified by mesoscale eddies in the upstream KE region, a double- (single-) branch jet can respond to the appearance of the KED^- (KED^+) mode. However, it is difficult to infer the cause and effect relationship among the KED mode, KE jet, and EKE if a yearly mean is used. Thus, to explore the association of the EKE variability with the KED mode and KE jet, it is necessary to examine the time evolution of the KED mode, KE jet, and EKE using the monthly mean data.

3.2 Monthly evolution of the spatial structures of KED mode, KE jet, and EKE

It is useful to use the monthly mean data to examine the spatiotemporal evolution of the KED and its relationship with the KE jet and mesoscale eddy activity in the upstream KE region because the yearly mean result cannot tell us their causal relationship. Here, we define the difference of the area-averaged monthly mean SSH anomaly between two regions: 141° E–153°E, 32° N–35° N and 141° E–153° E, 35° N–38° N as a monthly mean KED index to reflect the phase and strength of the monthly mean KED, while the KE jet and EKE strengths are defined in Section 2. A power spectral calculation reveals that the monthly mean KED exhibits different dominant periods of 1.5, 2.3, 3.8, and 10 years (not shown). While the 2.3 and 3.8 year periods of the KED mode may be attributed to the ENSO modulation, its 10-year period may come from the Pacific Decadal Oscillation (PDO) modulation (Ceballos et al. 2009). Thus, the KED mode may have an intrinsic period of 1.5 years, although it exhibits longer time periods under the ENSO and PDO modulations.

We pick 6 KED^+ (4 KED^-) events during 1993–2010 if the normalized monthly mean KED index is greater (less) than 0.4 (−0.4) standard deviation persisting for at least eight consecutive months. Obviously, the number of the strong KED^- (KED^+) events obtained from a monthly mean definition is not identical to that of WWJ (SNJ) events from a yearly mean definition although they are identified as corresponding to the

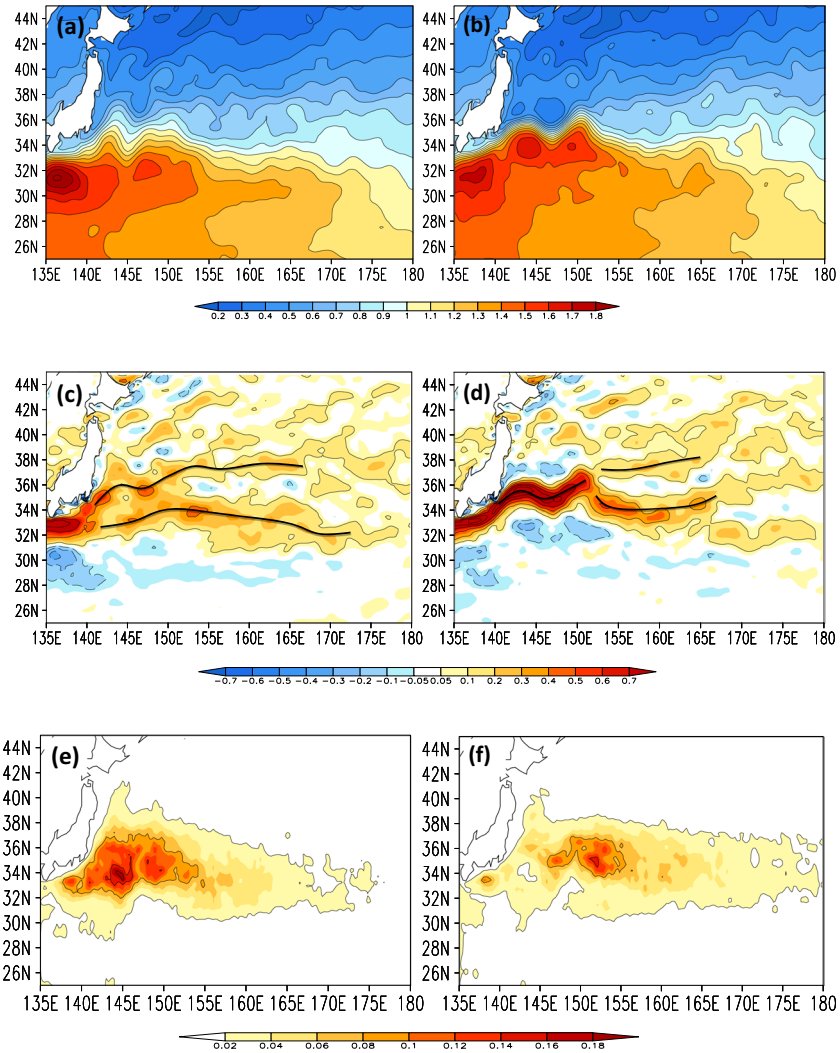

Fig. 1 **a**, **b** Average fields of yearly mean SSH (unit: m); **c**, **d** zonal current (unit: m s^{-1}); and **e**, **f** EKE (unit: m^2 s^{-2}) for WWJ (**a**, **c**, **e**; *left*) and SNJ (**b**, **d**, **f**; *right*) events. In each panel, the *red* (*blue*) denotes the high (low) value region

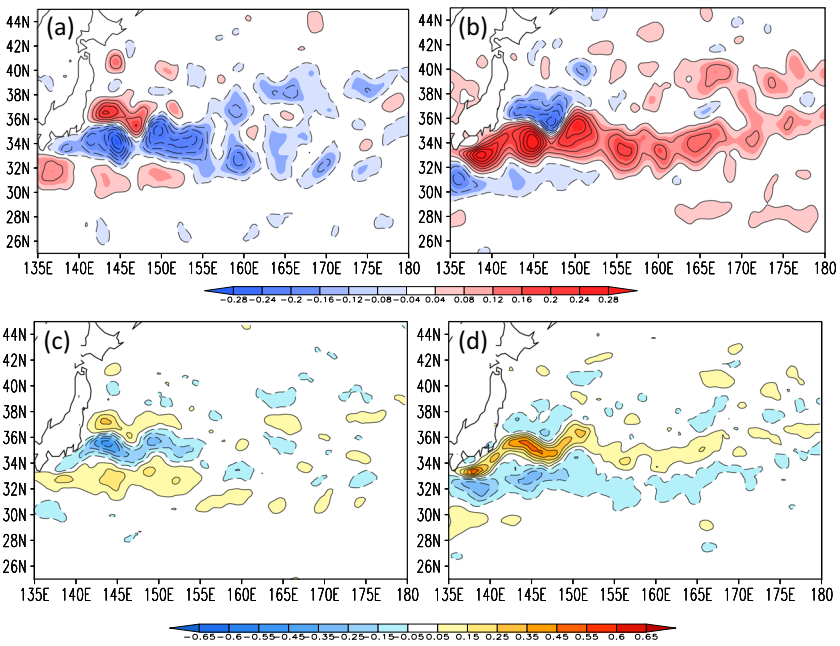

Fig. 2 **a**, **b** Average fields of yearly mean SSH (unit: m) and **c**, **d** zonal current anomalies (unit: m s^{-1}) for WWJ (**a**, **c**; *left*) and SNJ (**b**, **d**; *right*) events, in which the *red* (*blue*) denotes the positive (negative) anomaly region that exceeds the 99 % confidence level for a two-sided Student's *T* test. The effective degree of freedom is 4 (3) for WWJ (SNJ) events

KED$^-$ (KED$^+$) events. Here, we define the peak of each KED event as lag 0 month. The composite monthly mean SSH anomaly fields are shown in Fig. 3 for two phases of the KED mode during its life cycle (from lag −6 to 4 months). A dominant negative-over-positive SSH dipole anomaly resembling a KED$^+$ mode is seen in the upstream KE region, which undergoes a growth during the period from lag −6 to 0 months and then a decay from lag 0 to 4 months (Fig. 3a). In contrast, the growth and decay of a positive-over-negative SSH dipole anomaly that resembles a KED$^-$ mode are seen

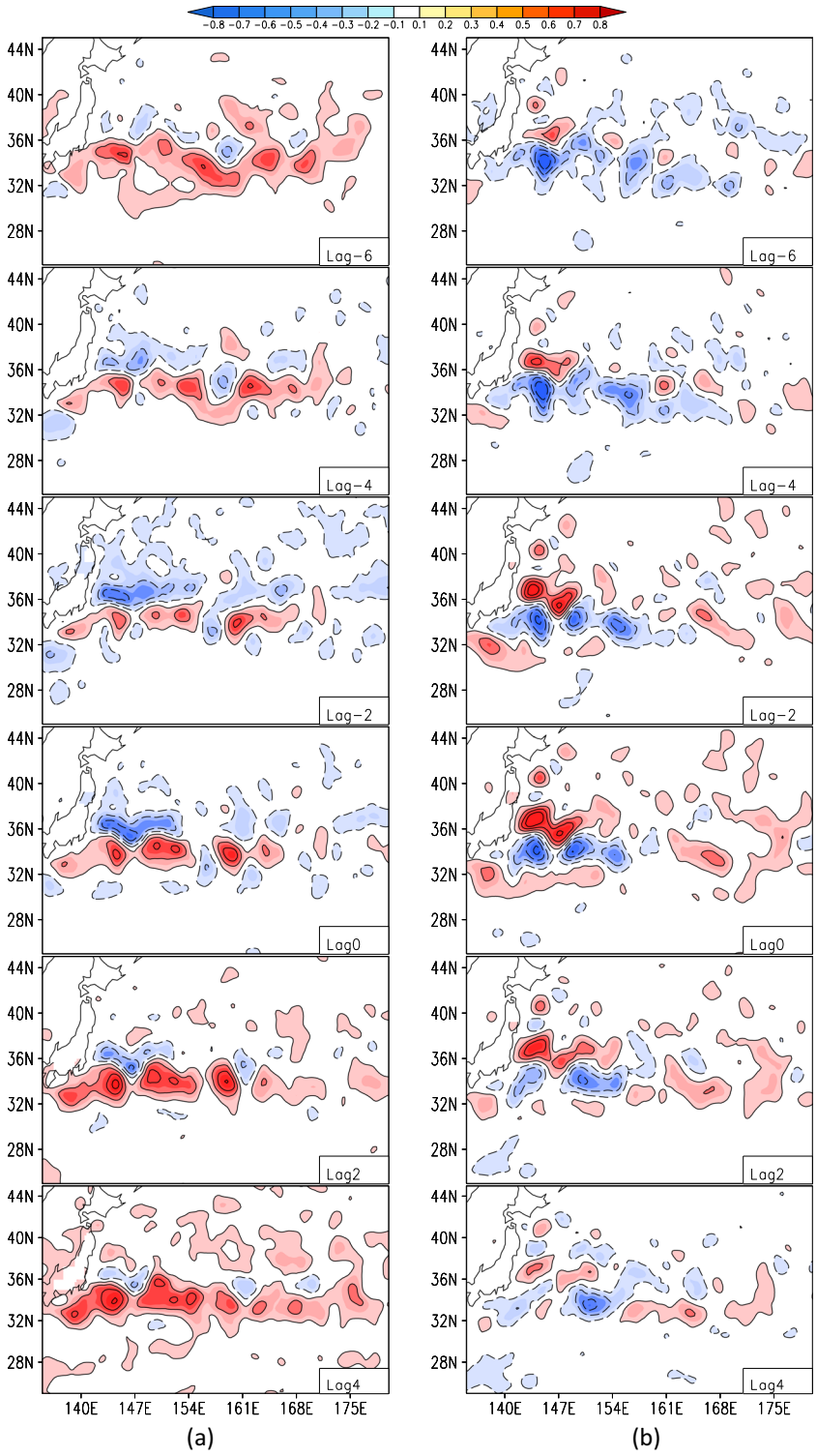

Fig. 3 Time evolution of composite monthly SSH anomalies (unit: m) for **a** KED$^+$ (*left*) and **b** KED$^-$ (*right*) modes. The positive (negative) SSH anomaly is marked with *red* (*blue*)

in Fig. 3b during the period from lag −6 to 4 months. To examine whether the variation of the KE current is an adjustment of the zonal geostrophic current to the KED mode, it is necessary to perform a composite of monthly mean sea-surface zonal current and show its result in Fig. 4 for two phases of the KED mode. It is seen that the KE current is intensified to establish the strongest single-branch jet structure at lag 0 month (Fig. 4a) when the KED^+ mode reaches its peak (Fig. 3a at lag 0 month). In contrast, the KE current is weakened to establish the clearest double-branch jet structure at lag

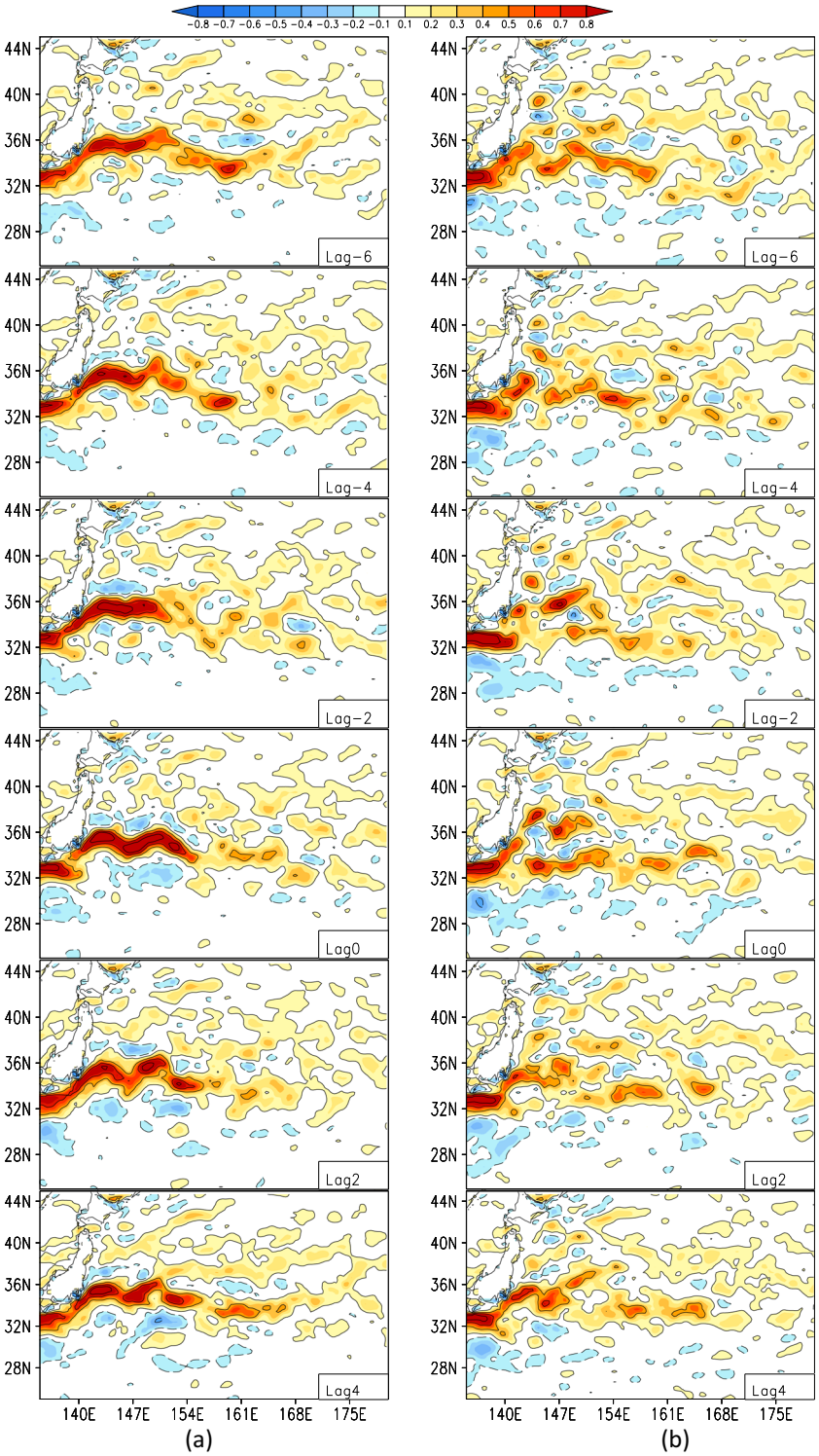

Fig. 4 Time evolution of composite monthly sea-surface zonal current (unit: m s^{-1}) for **a** KED^+ (*left*) and **b** KED^- (*right*) modes. The positive (negative) value is marked with *red* (*blue*)

0 month (Fig. 4b) as the KED$^-$ mode has the largest intensity (Fig. 3b at lag 0 month). Such a jet change is actually an adjustment of the zonal geostrophic current to an enhanced KED mode. Thus, when the KED mode occurs, a double-branch or (single-branch) jet can be established in the upstream KE region for the KED$^-$ (KED$^+$) mode, leading to a large (small) meandering of the KE jet.

To understand the relationship between the monthly EKE variation and the phase of the monthly mean KED mode, it is useful to plot the horizontal distribution of the composite monthly EKE anomaly in Fig. 5 for the two phases of the KED mode. Note that the EKE anomaly for each month is defined as a deviation of its value from its climatogical mean value. We can see from Fig. 5 that the EKE is weakened in the upstream KE region from lag −6 to 0 months as the KED$^+$ mode intensifies (Fig. 5a). During the large amplitude period of the KED$^+$ mode from lag −4 to 2 months, the weakening of this EKE is evident in the upstream KE region, but not in the downstream region. The main cause of this is that the large EKE is shifted to the downstream side of the KE region due to an enhanced eastward advection during the KED$^+$ period. In Fig. 5b, we also see that the EKE is gradually intensified in the upstream KE region from lag −6 to 0 months as the KED$^-$ mode is intensified, in contrast with the result of the KED$^+$ mode. Because the intensifying (weakening) of the EKE accompanies the growth of the KED$^-$ (KED$^+$) mode, it is inferred that the different deformation field of the KED mode for the different phase may contribute to the different variation of the EKE in the upstream KE region, although the mean flow shear (instability) and topography initiate small-scale eddies. This is possible because the large-scale dipole deformation field is able to alter the kinetic energy of small-scale eddies during their interaction in the turbulent theory, even though the large-scale dipole mode is driven by small-scale eddies. This viewpoint will be further indicated in Section 4 using a new eddy-dipole mode interaction theory. The interesting readers refer to the review paper of Holloway (2010) on this aspect.

It is also useful to examine the evolution of the monthly KED, EKE strength, and jet width indices in order to understand their relationship. We show the time series of the normalized composite monthly KED, EKE strength, and jet width indices in Fig. 6. It is seen from Fig. 6 that the regional-mean EKE strength averaged over the region (141° E–153° E, 32° N–38° N) increases (decreases) (Fig. 6b) as the KED$^-$ (KED$^+$) mode strengthens (Fig. 6a). Thus, there is an opposite variation between the EKE strength and the phase of the KED mode. It is further shown that for the KED$^-$ mode the EKE reaches its largest intensity at the peak of the KED$^-$ (lag 0 month) (dashed line in Fig. 6b), while the EKE seems to reach its weakest value at the peak of the KED$^+$ mode (solid line in Fig. 6b). These results demonstrate that the variation of the EKE in the upstream KE region depends strongly on the phase and strength of the KED mode. Moreover, we can see that the KE current tends to form a wide (narrow) jet event when the KED$^-$ (KED$^+$) mode grows, because the jet width index has a relatively large positive (negative) value (Fig. 6c). As noted below, the variation of the jet width or the transition between the WWJ and SNJ events is a natural result of the phase change in the intensified KED mode. However, how the KED mode changes the EKE is not clear. Below, this problem will be further examined using a new eddy-dipole mode interaction theory presented below.

4 The eddy-dipole mode interaction model and inverse energy cascades

4.1 Eddy-dipole mode interaction model

To understand the relationship between the KED mode and EKE variability, it is useful to construct an eddy-dipole mode interaction model to describe the variation of the EKE as the KED mode varies. As we can see from the above results, the KED mode has the zonal scale of 1000 km (Fig. 2a, b). Some studies also revealed that mesoscale eddies are often of nearly 200 km scale in the KE region (Waseda et al. 2002). Here, following the work of Chelton et al. (2011), the radius of mesoscale eddies in the KE region can be calculated using the Okubo-Weiss parameter. It is easily found that the mean radius of mesoscale eddies in the KE region is about 45 km, thus corresponding to a diameter of 90 km. This eddy scale is basically consistent with that estimated by Chelton et al. (2011), their Fig. 12), who found that the eddy has a scale of about 100 km near 30°N and a smaller scale to its north. Thus, the KED mode and KE eddies are approximately zonal separable. In this case, we may assume that there is a zonal scale separation between the KED mode and mesoscale eddies. This assumption is the so-called scale separation assumption (Luo 2000, Luo and Li, 2000; Luo et al. 2014, 2015). Although some studies revealed that baroclinic processes such as eddy stresses associated with buoyancy are also important for the KE variability (Berloff et al. 2007a), the KE current is approximately barotropic above the 1000 m depth (Pierini 2006; Pierini et al. 2009). Such a vertical structure allows us to use the RGSW equations to construct an eddy-dipole mode interaction model to diagnose the mutual relationship between the time-varying KED mode and the EKE change in the upstream KE region. Using the RGSW equations is reasonable at least for investigating the dynamical mechanism of the KE variability if the KE current is assumed to be composed of a thin upper active layer superimposed on a much deeper quiescent lower layer, as done in Pierini

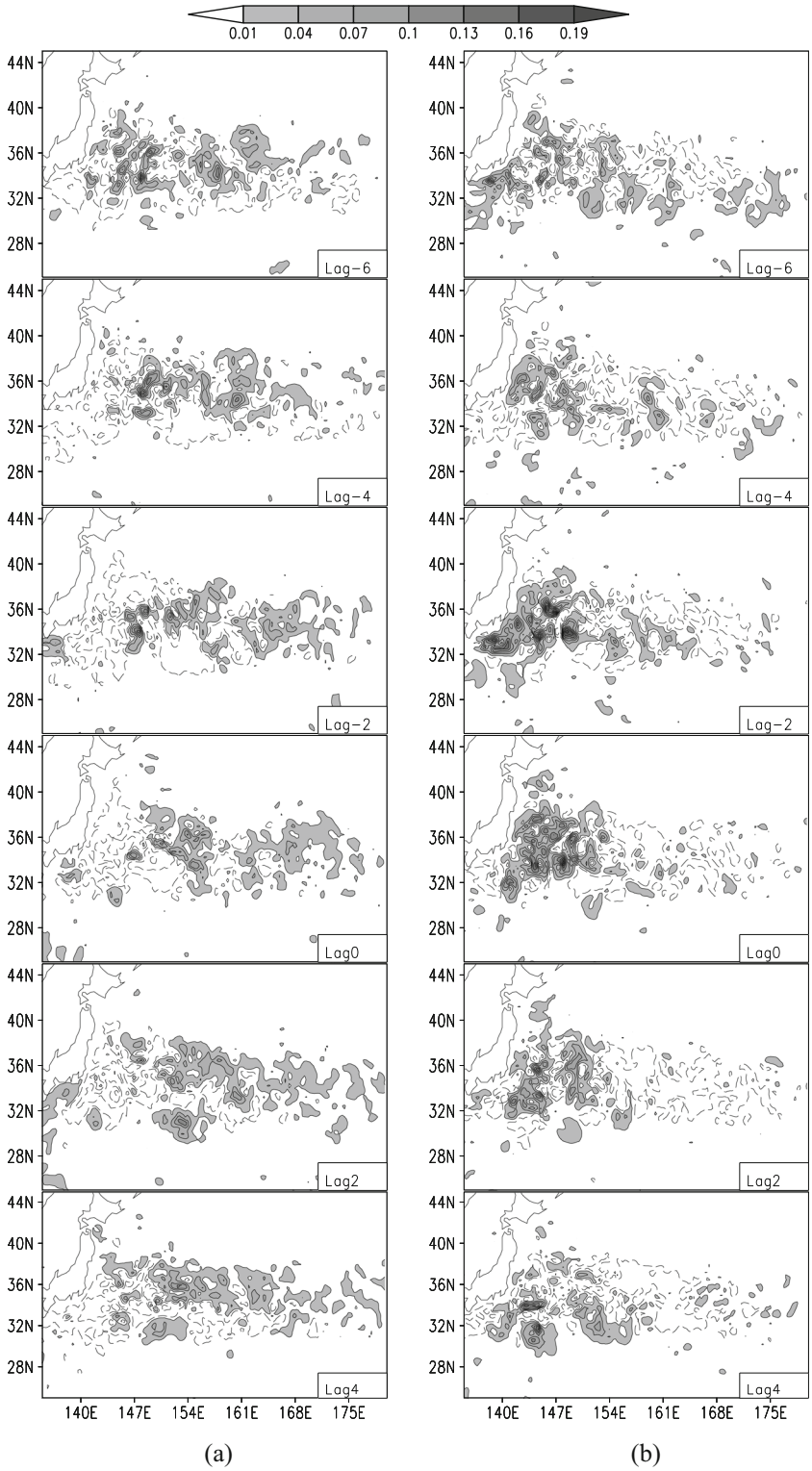

Fig. 5 Composite monthly EKE anomaly (unit: $m^2\ s^{-2}$) for **a** KED^+ (*left*) and **b** KED^- (*right*) modes. The dashed (*solid*) region represents the negative (positive) EKE anomaly

(2006). This RGSW model has been widely used to investigate the decadal variability of the KE system and associated dynamics (Pierini 2006; Pierini et al. 2009; Sasaki et al. 2013). In this paper, we used the RGSW model to test our hypothesis by neglecting baroclinic processes such as the buoyancy flux (Berloff et al. 2007a, b), because our attention is focused on the sea-surface eddy activity in the upstream KE region.

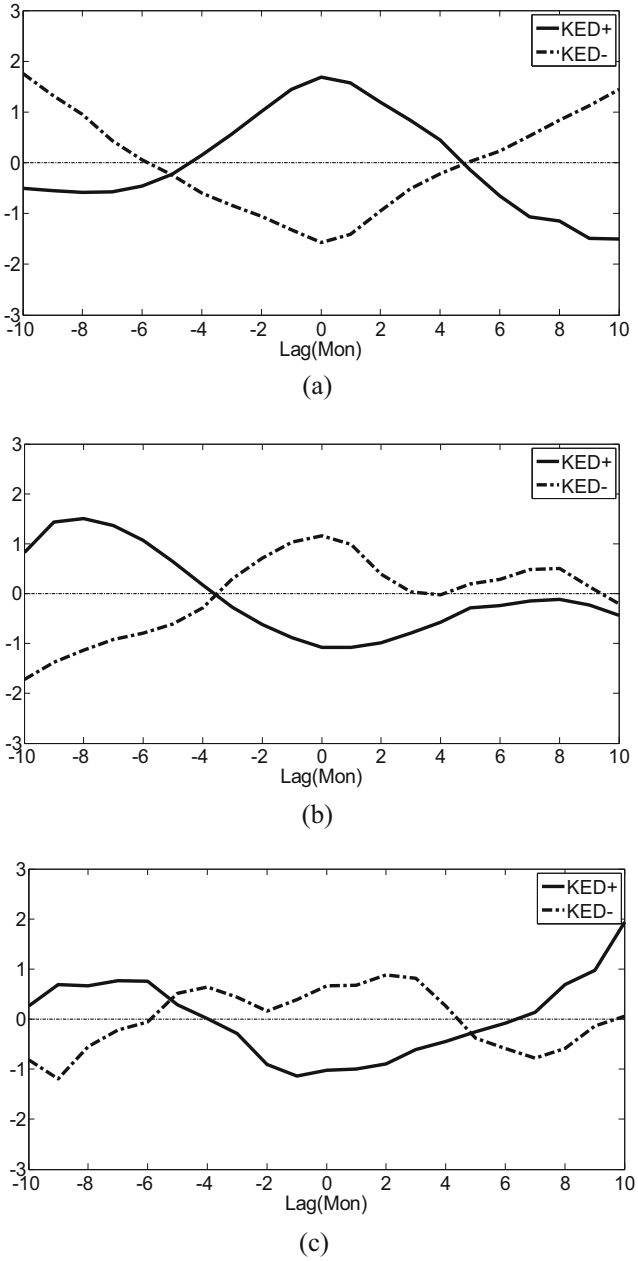

Fig. 6 Monthly variations of **a** normalized composite KED strength, **b** EKE strength, and **c** jet width indices for 6 KED^{+} (solid) and 4 KED^{-} (dashed) events. The *y-coordinate* denotes the normalized index

The RGSW equations are expressed as (Cushman-Roisin 1986)

$$\frac{\partial u}{\partial t}+u\frac{\partial u}{\partial x}+v\frac{\partial u}{\partial y}-fv=-\frac{\partial \phi}{\partial x} \tag{1a}$$

$$\frac{\partial v}{\partial t}+u\frac{\partial v}{\partial x}+v\frac{\partial v}{\partial y}+fu=-\frac{\partial \phi}{\partial y} \tag{1b}$$

$$\frac{\partial \phi}{\partial t}+\frac{\partial(\phi u)}{\partial x}+\frac{\partial(\phi v)}{\partial y}=0 \tag{1c}$$

where $\phi=g'h$ is the gravity potential, h is the upper layer thickness, g' is the reduced gravity, f is the Coriolis parameter and $\boldsymbol{v}=(u,v)$ is the horizontal velocity vector. Note that Eqs. (1a–1c) govern the evolution of a two-layer system in which the deep lower layer is approximately at rest. This assumption is held for the oceanic motions above the 1000 m depth.

Assuming that the oceanic current $\boldsymbol{v}=(u,v)$ is divided into large-scale ($\boldsymbol{V}=(U,V)$, Φ) dipole modes and mesoscale ($\boldsymbol{v}'=(u',v')$, ϕ') eddies. Under both the quasi-geostrophic and scale separation assumptions (Luo 2000; Luo and Li 2000, Luo et al. 2014), we obtain the equations for quasi-geostrophic vorticity and the eddy kinetic energy generation (Luo et al. 2015, see their Appendix)

$$\frac{\partial q}{\partial t}+J(\psi,q)+\beta\frac{\partial \psi}{\partial x}+f\nabla\cdot\boldsymbol{V}=-\nabla\cdot\left(\boldsymbol{v}'q'\right)_P \tag{2a}$$

$$\frac{\partial e}{\partial t}=-\boldsymbol{V}\cdot\nabla e+\boldsymbol{E_m}\cdot\boldsymbol{D}+\mathrm{OTH} \tag{2b}$$

where $q=\partial V/\partial x-\partial U/\partial y$, $\boldsymbol{V}=(U,V)=(-\partial\psi/\partial y,\partial\psi/\partial x)$, $\boldsymbol{v}'=(u',v')$ is the horizontal eddy current velocity with the relative vorticity $q'=\partial v'/\partial x-\partial u'/\partial y$, $e=(u'^2+v'^2)/2$ is the high-frequency eddy kinetic energy (EKE), $\boldsymbol{E_m}=(E_{mx},E_{my})=((v'^2-u'^2)/2,-u'v')$ is the $\boldsymbol{E_m}$ vector consisting of the elements of the anisotropic part of the instantaneous horizontal velocity correlation tensor (Mak and Cai 1989), and $\boldsymbol{D}=\left(D_x,D_y\right)=\left(\frac{\partial U}{\partial x}-\frac{\partial V}{\partial y},\frac{\partial V}{\partial x}+\frac{\partial U}{\partial y}\right)$ is the large-scale strain tensor induced by the KED mode that reflects the large-scale deformation field of the KED mode. It should be pointed out that in Eq. (2a) $\nabla\cdot(\boldsymbol{v}'q')_P$ denotes the large-scale component of $\nabla\cdot(\boldsymbol{v}'q')=\nabla\cdot\boldsymbol{D_e}$ ($\boldsymbol{D_e}=(u'q',v'q')=(-\boldsymbol{k}\cdot\nabla\times\boldsymbol{E_m},\nabla\cdot\boldsymbol{E_m})$), close to the zonal scale of the KED mode, $\boldsymbol{k}$ is the unit vector in the vertical direction, and OTH represents a higher order term arising from the nonlinear interaction of mesoscale eddies themselves which is smaller and assumed to be negligible compared to other terms in Eq. (2b) (Luo et al. 2015). The boundary conditions in zonal and meridional directions are not needed for the derivation of Eqs. (2a and 2b), but solving Eqs. (2a and 2b) needs the boundary conditions. On the other hand, it should be pointed out that Eq. (2a) is the reduced gravity shallow water quasi-geostrophic vorticity equation because the quasi-geostrophic assumption is applied in the derivation of Eqs. (2a and 2b).

Equations (2a and 2b) are identical to the eddy-wave interaction equation derived by Luo et al. (2015). It should be noted that Eq. (2a) represents the large-scale vorticity equation with an eddy vorticity forcing term $\nabla\cdot(\boldsymbol{v}'q')_P$ having a low-frequency timescale, which describes how the evolution of the low-frequency KED mode is driven by high-frequency eddies. While Eq. (2b) describes how the spatiotemporal variation of the EKE depends on the time-dependent deformation field of the KED mode, Eq. (2a) actually describes an inverse

energy cascade from eddy to KED scales. Because Eqs. (2a and 2b) are a coupled equation, Eq. (2b) can reveal that the EKE exhibits a decadal variation if the KED mode in Eq. (2a) ($\boldsymbol{V}$ and $\boldsymbol{D}$ vectors in Eq. (2b)) undergoes a decadal change under the PDO or decadal turbulent oscillator modulation. This eddy-dipole mode interaction equation is different from the previous models. In previous eddy-mean flow interaction models, the small-scale eddy equation vanishes because a time mean is applied (Hoskins et al. 1983; Holopainen and Fortelius 2007). In this case, the eddy-mean flow interaction equation is only described by $\frac{\partial \overline{q}}{\partial t} + J\left(\overline{\psi}, \overline{q}\right) + \beta\frac{\partial \overline{\psi}}{\partial x} + f\nabla\cdot\overline{\boldsymbol{V}} = -\nabla\cdot\overline{\left(\boldsymbol{v}'q'\right)}$, where the overbar denotes a time mean during a period equal to or longer than the life times of high-frequency eddies.

In Eq. (2b), $-\boldsymbol{V}\cdot\nabla e$ reflects the change in the EKE induced by the large-scale advection, whereas $\boldsymbol{E_m}\cdot\boldsymbol{D}$ reflects the EKE change induced by the deforming field of the KED mode. It is also useful to rewrite $\boldsymbol{E_m}\cdot\boldsymbol{D}$ as $\boldsymbol{E_m}\cdot\boldsymbol{D} = E_{mx}D_x + E_{my}D_y$, where $E_{mx}D_x$ and $E_{my}D_y$ represent the stretching and shearing deformation terms induced by the KED mode, respectively. By examining the magnitude and distribution of the terms $-\boldsymbol{V}\cdot\nabla e$, $E_{mx}D_x$, $E_{my}D_y$, and $\boldsymbol{E_m}\cdot\boldsymbol{D}$, it becomes feasible to understand how the KED mode modulates the EKE in the upstream KE region. Thus, Eqs. (2a and 2b) can tell us how the KED mode and EKE are dependent on each other. In the next subsection, we will explore whether the mesoscale eddies contribute to the intensification of the KED mode by defining and calculating an eddy-induced dipole index before how the KED mode modulates the EKE in the upstream KE region is examined.

4.2 Instantaneous contributions of high-frequency eddies to the KED mode

To understand the role of high-frequency or mesoscale eddies in the KED mode, it is reasonable to calculate the eddy-induced large-scale streamfunction tendency ψ_P^{vort} that satisfies $\left(\frac{\partial q}{\partial t}\right)_{TE} = \frac{\partial q}{\partial t} + J(\psi, q) + \beta\frac{\partial \psi}{\partial x} + f\nabla\cdot\boldsymbol{V} = \nabla^2\psi_P^{\mathrm{vort}} = -\nabla\cdot\left(\boldsymbol{v}'q'\right)_P$ or $\psi^{vort} = \nabla^{-2}[-\nabla\cdot(\boldsymbol{v}'q')]$ during the KED life cycle parallel to the definition $\psi^{\mathrm{vort}} = -\nabla^{-2}\left[\nabla\cdot\left(\boldsymbol{v}'q'\right)\right]$ of Holopainen and Fortelius (1987), where ψ_P^{vort} is the large-scale component of ψ^{vort}. If $\left(\frac{\partial q}{\partial t}\right)_{TE} = \frac{\partial \nabla^2\psi_{TE}}{\partial t} = \nabla^2\psi_P^{\mathrm{vort}}$ is defined, then $\frac{\partial \psi_{TE}}{\partial t} = \psi_P^{\mathrm{vort}}$ represents the eddy-induced large-scale streamfunction tendency and actually reflects the net effect of high-frequency eddies on the KED mode, which reflects the eddy-induced large-scale streamfunction tendency that affects the evolution of the KED mode (Luo et al. 2015).

Using a quasi-geostrophic approximation $\nabla\cdot\boldsymbol{V} = -\frac{f}{{c_0}^2}\frac{\partial \psi}{\partial t}$ (where ${c_0}^2 = g'H$ and H is the mean depth of the upper layer fluid), Eq. (2a) is reduced to $\left(\frac{\partial q}{\partial t}\right)_{TE} = \frac{\partial\left(q-\lambda^2\psi\right)}{\partial t} + J(\psi, q+\beta y) = \nabla^2\psi_P^{\mathrm{vort}} = -\nabla\cdot\left(\boldsymbol{v}'q'\right)_P$, where $\lambda = \frac{f}{c_0}$. It is clear that when the eddy vorticity forcing term $\nabla\cdot(\boldsymbol{v}'q')_P$ vanishes, we have a simplified vorticity equation of $\frac{\partial\left(q-\lambda^2\psi\right)}{\partial t} + J(\psi, q+\beta y) = 0$. In this equation, the time derivative term $\frac{\partial\left(q-\lambda^2\psi\right)}{\partial t}$ of the KED mode is balanced by its advection term $J(\psi, q+\beta y)$. This equation has a stationary or uniformly translating, shape preserving (or modons) solution as obtained by Stern (1975) and Larichev and Reznik (1976), which is not changed with time. Such a solution corresponds to a free mode because the potential vorticity and its streamfunction satisfy a linear relationship. However, the KED mode does not possess such a feature because our calculation indicates that there is $J(\psi, q+\beta y) \neq 0$ during the KED life cycle (not shown), thus indicating that the KED mode is a forced mode. As shown by Fig. 3, the amplitude of the KED mode is always changed with time; thus, it is not in a balance state even when its amplitude is rather large. This point can also be further seen from Fig. 6a. Thus, in the vorticity equation of $\left(\frac{\partial q}{\partial t}\right)_{TE} = \frac{\partial\left(q-\lambda^2\psi\right)}{\partial t} + J(\psi, q+\beta y) = \nabla^2\psi_P^{\mathrm{vort}} = -\nabla\cdot\left(\boldsymbol{v}'q'\right)_P$, $-\nabla\cdot(\boldsymbol{v}'q')_P$ may be considered as a forcing of the KED mode that satisfies the equation $\frac{\partial\left(q-\lambda^2\psi\right)}{\partial t} + J(\psi, q+\beta y) = 0$. This point can be indicated below.

Although Eqs. (2a and 2b) are used to diagnose the contribution of mesoscale eddies to the KED mode and how the KED mode modulates the EKE in the upstream KE region, the boundary conditions of ψ^{vort} must be specified to obtain its solution. To obtain ψ^{vort}, we assume that $\psi^{vort} = 0$ for a rigid condition in the meridional direction with a sufficient large width and $\psi^{vort} = 0$ at the Japan Island coast and at a sufficient long distance to the east of the KE region in the zonal direction. It is easy to obtain the spatial distribution of ψ^{vort} in a narrow region around the KE region once it is obtained in a large region around the KE. Such a treatment is acceptable because mesoscale eddies disappear at a large domain boundary.

As revealed by Eq. (2a), the KED mode is mainly changed by the large-scale component of eddy vorticity flux divergence $\psi_P^{\mathrm{vort}} = \nabla^{-2}\left[-\nabla\cdot\left(\boldsymbol{v}'q'\right)_P\right]$, although it is also affected by term $J(\psi, q+\beta y)$. As noted by Holopainen and Fortelius (1987), the time-mean eddy vorticity flux divergence term $-\nabla\cdot\left(\boldsymbol{v}'q'\right)$ plays a very important role in the maintenance of time-mean large-scale anomalies, while it is a small term compared to other terms such as $J(\psi, q)$ and $\beta\frac{\partial \psi}{\partial x}$. Here, to quantify the role of mesoscale eddies, it is useful to construct an eddy-induced dipole index. While ψ^{vort} in $\psi^{vort} = \nabla^{-2}[-\nabla\cdot(\boldsymbol{v}'q')]$ is not identical to ψ_P^{vort}, we may approximate ψ_P^{vort} as the zonal average of ψ^{vort} in the upstream KE region. Here, we define $BI_e(t) = [\psi^{vort}]_S - [\psi^{vort}]_N$ as an eddy-induced dipole index, where $[\psi^{vort}]_S$ and $[\psi^{vort}]_N$ represent the regional average of ψ^{vort} over two sides (141° E–153° E, 32° N–35° N and 141° E–153° E, 35° N–38° N) of the KED mode, respectively. Such

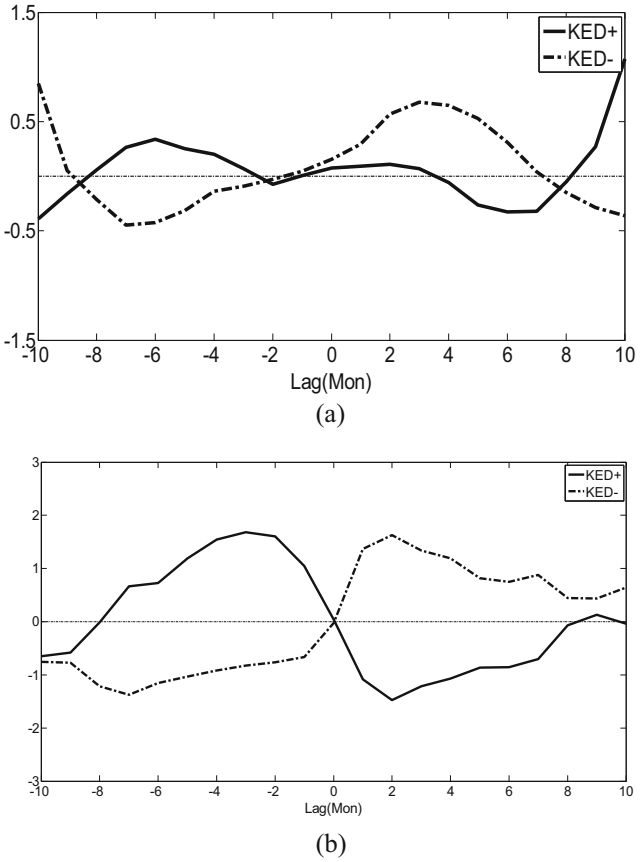

Fig. 7 Monthly variations of normalized **a** eddy-induced dipole index $BI_e(t)$ and **b** KED variation rate index $BT(t)$ for KED^+ (*solid*) and KED^- (*dashed*) modes. The *y-coordinate* denotes the normalized index

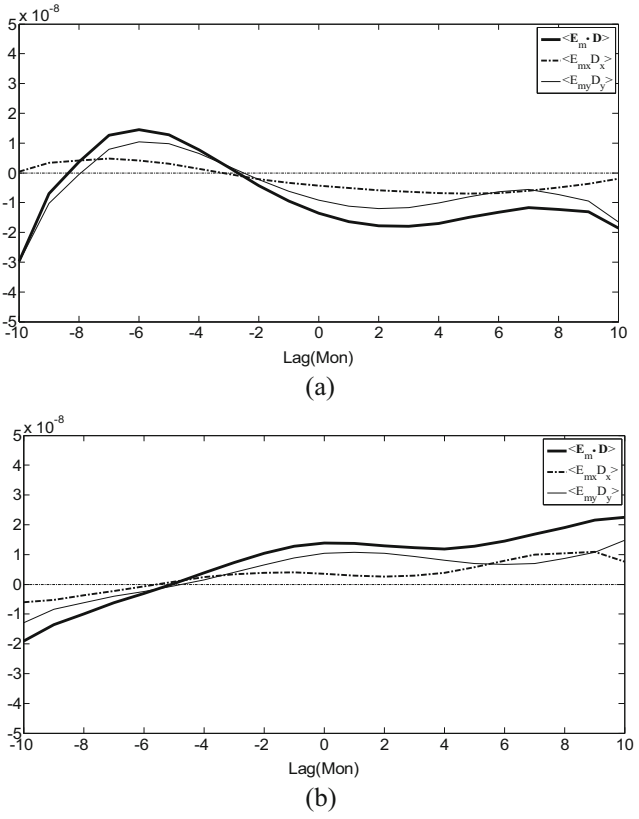

Fig. 9 Time variation of the composite monthly $\langle \boldsymbol{E_m} \cdot \boldsymbol{D} \rangle$, $\langle E_{mx} D_x \rangle$, and $\langle E_{my} D_y \rangle$(*y-coordinate* and its unit: $m^2\ s^{-3}$) averaged over the region (141° E–153° E, 32° N–38° N) for **a** $KED^+$and **b** KED^- modes

a definition is reasonable because the eddy vorticity forcing term ψ_P^{vort} must be required to have a dipole structure to generate the variation of the KED mode. Because in both $\left(\frac{\partial q}{\partial t}\right)_{TE} = \frac{\partial\left(q-\lambda^2\psi\right)}{\partial t} + J(\psi, q+\beta y) = \nabla^2\psi_P^{\mathrm{vort}}$ and $q = \nabla^2\psi \propto -\psi$, we can have $\frac{\partial\psi}{\partial t} \sim \psi_P^{\mathrm{vort}}$. In this case, it is useful to construct an index describing the variation rate of the KED mode. We define

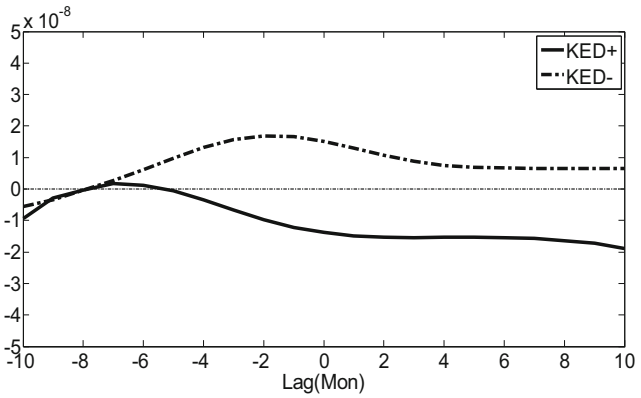

Fig. 8 Time variation of the composite monthly $-\langle \boldsymbol{V} \cdot \nabla e \rangle$ (*y-coordinate* and its unit: $m^2\ s^{-3}$) averaged over the region (141° E–153° E, 32° N–38° N) for two phases of the KED mode

$BT = \left[\frac{\partial\psi}{\partial t}\right]_S - \left[\frac{\partial\psi}{\partial t}\right]_N$ as an index to describe the variation of the KED mode, where $\left[\frac{\partial\psi}{\partial t}\right]_S$ and $\left[\frac{\partial\psi}{\partial t}\right]_N$ represent the values of $\frac{\partial\psi}{\partial t}$ averaged over two regions (141° E–153° E, 32° N–35° N and 141° E–153° E, 35° N–38° N, respectively).

Because the value of BT is proportional to BI_e, the mesoscale eddies are meant to be able to amplify the KED^- (KED^+) mode when $BI_e < 0$ ($BI_e > 0$). But the opposite role is seen for $BI_e > 0$ ($BI_e < 0$). Thus, the eddy-induced variation of the KED mode can be approximately described by the sign and variation of the BI_e index. Here, we only present the monthly evolution of the normalized indices $BI_e(t)$ and $BT(t)$ instead of plotting $\frac{\partial q}{\partial t}$ to examine the importance of high-frequency eddies in driving the KED mode.

Figure 7 shows the time series of $BI_e(t)$ and $BT(t)$ for two phases of the KED mode. It is seen from the time variation of $BI_e(t)$ in Fig. 7a that for the KED^- mode (dashed line in Fig. 7a) $BI_e(t)$ is negative between lag −9 and −1 months and positive between lag −1 and +7 months. Thus, the eddy vorticity flux forcing can strengthen the KED^- mode during the period from lag –9 to −1 months, but favor its decay from lag −1 to +7 months. For the KED^+ mode (solid line in Fig. 7a), $BI_e(t)$ is positive between lag −8 and −2 months or weakly positive between lag −1 and 3 months, and strongly

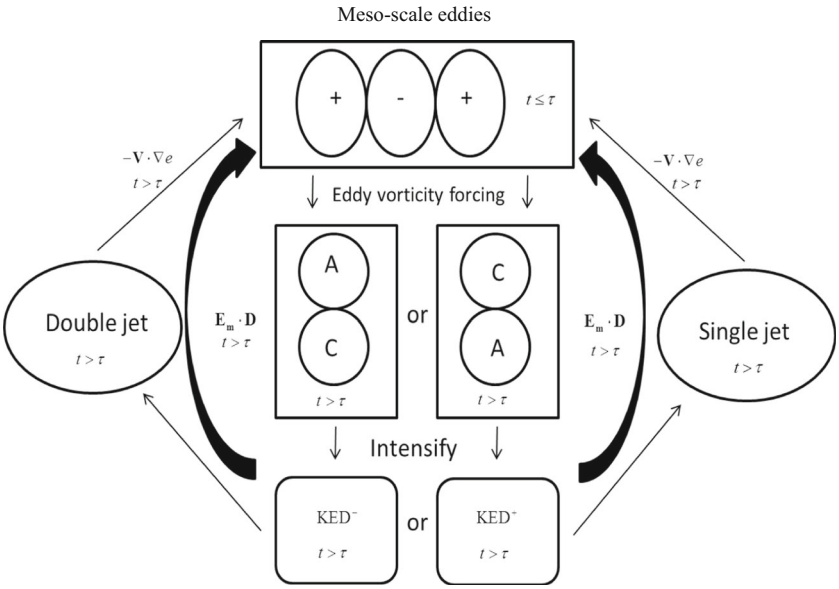

Fig. 10 Idealized schematic diagram of the mesoscale eddies reinforcing both the KED mode and KE jet and their feedback on mesoscale eddies. The monopole mesoscale eddies have a period $t \le \tau$ ($\tau = 300$ daysis a threshold) and induce the dipole eddy vorticity forcing $\nabla \cdot (\overline{v'q'})_P$ with a period $t > \tau$. The sign "+ (−)" denotes the anticyclonic (cyclonic) eddy and "A (C)" represents anticyclonic (cyclonic) forcing

negative between lag +4 and +8 months. To some extent, the growth (decay) of the KED$^+$ mode can crudely be explained by the positive (negative) value of $BI_e(t)$. It is obvious that the variation of $BI_e(t)$ (Fig. 7a) is basically consistent with that of $BT(t)$ as shown in Fig. 7b. Thus, the variation of the vorticity forcing from mesoscale eddies in the upstream KE region can drive the evolution of the KED mode from the growth to decay. This process is the so-called inverse energy cascade from small to large scales in the upstream KE region as found in the high-resolution model simulation (Serazin et al. 2015). It should be pointed out that the time variation of $BI_e(t)$ is not exactly consistent with that of $BT(t)$ because there is $J(\psi, q + \beta y) \neq 0$ in the equation $\left(\frac{\partial q}{\partial t}\right)_{TE} = \frac{\partial\left(q - \lambda^2\psi\right)}{\partial t} + J(\psi, q + \beta y) = \nabla^2 \psi_P^{\text{vort}}$. Even so, this does not preclude the important role of mesoscale eddies in driving the KED mode evolution.

Although the above result reveals that mesoscale eddies can drive the KED mode in terms of Eq. (2a), how the variation of the KED mode affects the mesoscale eddy activity in the upstream KE region should be further understood according to Eq. (2b). In the next section, our emphasis will be placed on examining how the change in the deformation field of the KED affects the EKE field.

5 Roles of large-scale current advection and KED deformation field in the variation of eddy energy

5.1 Role of large-scale current advection

As shown in Eq. (2b), the EKE advection term $-\boldsymbol{V} \cdot \nabla e$ by large-scale horizontal currents of the KED mode and $\boldsymbol{E_m} \cdot \boldsymbol{D}$ by the KED deformation field can affect the eddy energy. Thus, in this subsection, we first examine the role of the EKE advection by large-scale currents.

We show the monthly evolution of $-\langle \boldsymbol{V} \cdot \nabla e \rangle$ in Fig. 8, where $\langle A \rangle$ denotes a regional average over 32° N–38° N and 141° E–153° E. It is seen that there is a significant weakening (strengthening) of the regional averaged EKE advection $-\langle \boldsymbol{V} \cdot \nabla e \rangle$ in the upstream KE region during the KED$^+$ (KED$^-$) growing phase. Thus, the weak (strong) EKE in the upstream KE region during the KED$^+$ (KED$^-$) period is in part attributed to the enhanced (weakened) EKE advection due to the enhanced (reduced) zonal current. However, as we will demonstrate in the next subsection, the KED deforming field also plays a very important role in the EKE variation.

5.2 Role of the KED deformation field in the eddy energy variation

We show the monthly variations of $\langle \boldsymbol{E_m} \cdot \boldsymbol{D} \rangle$, $\langle E_{mx} D_x \rangle$, and $\langle E_{my} D_y \rangle$ averaged over 32° N–38° N and 141° E–153° E in Fig. 9. It is found that for the KED$^+$ mode $\langle \boldsymbol{E_m} \cdot \boldsymbol{D} \rangle$ decreases from lag −6 to 7 months and becomes negative after lag −3 months. Moreover, we see that $\langle E_{mx} D_x \rangle$ and $\langle E_{my} D_y \rangle$ are negative after lag −3 months, even though $\langle E_{my} D_y \rangle$ is negatively larger than $\langle E_{mx} D_x \rangle$ during the period from lag −3 to +5 months (Fig. 9a). Thus, during the KED$^+$period, the kinetic energy of mesoscale eddies weakens by losing energy to the KED$^+$ shearing and stretching deformation fields.

During the KED$^-$ mode period $\langle E_{my} D_y \rangle$ is largely positive (thin solid line in Fig. 9b) during the period from lag −4 to +5 months, while the positive value of $\langle E_{mx} D_x \rangle$ is relatively small (dashed line in Fig. 9b). This demonstrates that the kinetic energy of mesoscale eddies in the upstream KE region

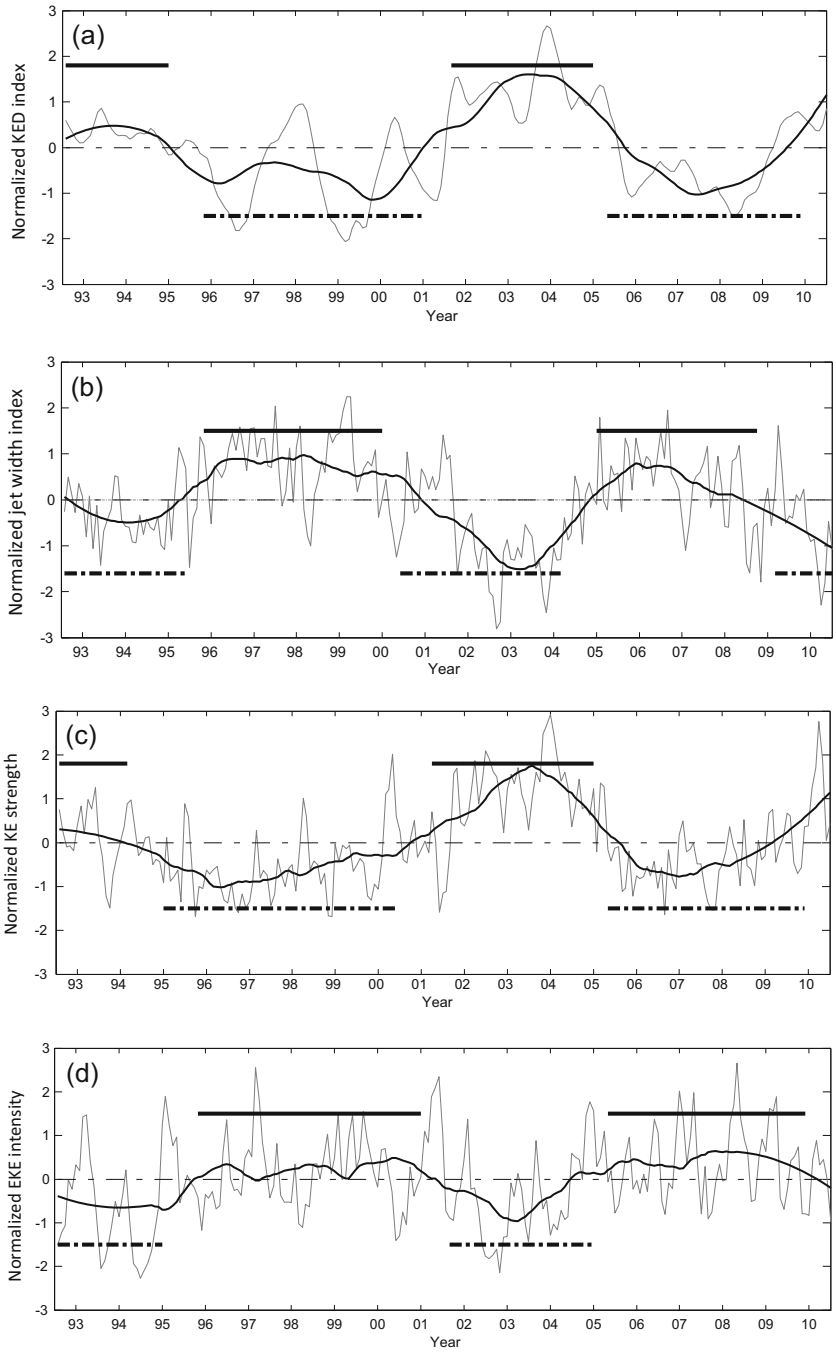

Fig. 11 Time series of normalized monthly mean **a** KED index, **b** jet width index, **c** KE strength, and **d** EKE intensity during the period from January 1993 to December 2010. The *solid line* denotes the 11-month smoothing curve

strengthens mainly by extracting energy from the KED$^-$ shearing and stretching deformation fields. This viewpoint is different from the inference of Qiu and Chen (2010), who emphasized the role of the KE current-topography interaction. Thus, the deformation field of the KED mode is important for the EKE change between the two phases of the KED mode. The EKE exhibits inevitably a well-defined decadal variation through changes in the zonal current and deformation field of the KED mode if the phase and strength of the KED mode undergo a decadal change under the PDO modulation.

6 Physical cause of the decadal variability of eddy kinetic energy

6.1 A physical explanation for the interaction among the KED mode, KE jet, and EKE on low-frequency timescales

As found above, the different horizontal advection and deformation field of the KED mode can induce the different variation of the EKE. Here, we present a physical explanation for

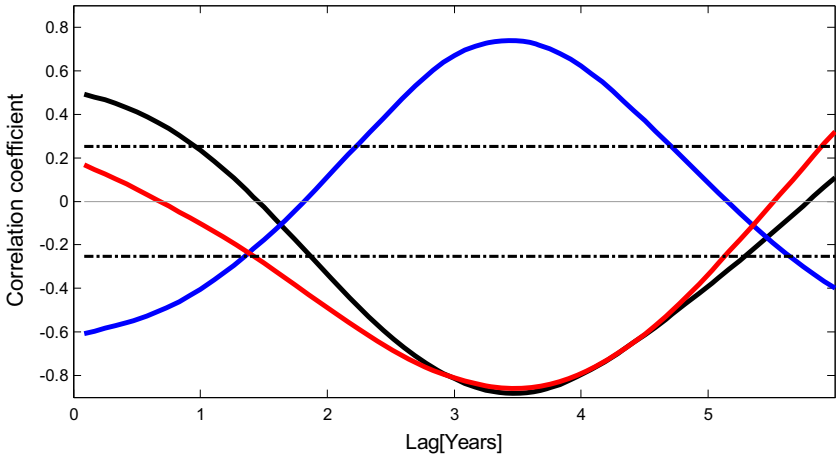

Fig. 12 Correlation coefficients between the PDO index and KED (*black*), jet (*red*), and EKE strengths (*blue*) indices after the 11-month smoothing. The *dot-solid line* denotes the 95 % confidence level

why the KED mode, KE jet, and EKE tend to have the same low-frequency period. An idealized schematic diagram is presented in Fig. 10 to understand their cause and effect relationship. Prior to the KED mode, the mesoscale eddies with timescales of $t \leq \tau$ (τ is the maximum duration of mesoscale eddies) have in general a monopole meridional structure. These eddies can induce a dipole eddy vorticity forcing $\nabla \cdot (\vec{v}'q')_P$ with a low-frequency period $t > \tau$ that drives the low-frequency KED mode to grow or decay, while its phase depends, to some extent, on the sign of arrival westward propagating signal associated with the PDO over the south side of the KE jet axis. When a KED$^-$ (KED$^+$) mode is intensified due to the dipole eddy vorticity forcing, a WWJ (SNJ) structure with a period $t > \tau$ is generated as a geostrophic balance. On the other hand, according to Eq. (2b), the mesoscale eddies are modulated by the KED mode through the large-scale advection $-\boldsymbol{V} \cdot \nabla e$ and KED deformation field $\boldsymbol{E_m} \cdot \boldsymbol{D}$, and thus, the EKE exhibits the same low-frequency timescale as those of the KED mode and the KE jet. In this case, the KED mode, KE jet, and EKE possess inevitably the same low-frequency period. In the next subsection, observational evidence will be provided to support this hypothesis.

6.2 Decadal modulation of the eddy kinetic energy by the decadal variation of the KED mode

In this subsection, we will present an observational evidence to support our physical explanation for why the EKE exhibits a decadal variability. It is useful to plot the time variations of the KED index, jet width index, KE strength, and EKE intensity during 1993–2010 in Fig. 11. It is seen that the KED index is negative during 1996–2001 and 2006–2009, but positive during 1993–1995 and 2002–2005 (Fig. 11a). For this case, KED$^-$ (KED$^+$) events are more frequent during 1996–2001 and 2006–2009 (1993–1995 and 2002–2005). As a result, the frequency of KED$^-$ (KED$^+$) events shows a clear decadal variation. Because the KED$^-$ (KED$^+$) event corresponds to the high (low) EKE level (Fig. 6b), the EKE exhibits inevitably a distinct decadal variation. This can be clearly seen from Fig. 11d. On the other hand, because each KED$^-$ (KED$^+$) mode corresponds to a wide (narrow) jet event as a geostrophic adjustment and because the frequency of the KED mode has a decadal change, the decadal variations of the jet width (Fig. 11b) and KE strength (Fig. 11c) are inevitably seen. Thus, the above results indicate that the KE jet and EKE exhibit inevitably decadal variations when the phase of the KED mode has a decadal change.

6.3 What determines the phase of the KED mode?

Although Qiu and Chen (2005, 2010) and Pierini (2014) found that the KE decadal variability is closely related to the PDO and North Pacific Oscillation (NPO), they did not mention that the decadal variation of the KE system is attributed to the decadal modulation of the KED mode by the PDO or NPO. Sasaki et al. (2013) also found that the SSH anomalies in the Central and East North Pacific driven by the PDO can reach the KE region. Here, we present a hypothesis that the phase of the KED mode is likely determined by the phase of the PDO. To confirm this hypothesis, it is useful to calculate the correlation coefficients of the KED mode, KE jet, and EKE strengths with the PDO index in Fig. 12. It is seen that the KED index has a maximum negative correlation of −0.88 with the PDO index at the 3.4-year time lag (black line in Fig. 12), while the EKE (KE jet) strength has a maximum positive (negative) correlation of 0.77 (−0.86) with the PDO index at the same time lag (blue and red lines in Fig. 12). This 3.4-year time lag reflects the need time of PDO-induced SSH anomalies propagating into the KE region from the East North Pacific. Thus, to some extent, the phase of the KED mode is mainly determined by the PDO and exhibits a decadal change. Because of the organization role of the KED mode (Figs. 8 and 9), the EKE exhibits inevitably a decadal variation depending on the phase and strength of the KED mode.

7 Conclusion and discussions

In this paper, by proposing the concept of large-scale dipole (KED) modes in the upstream KE region and defining a KED index, we have examined the mutual relation between the Kuroshio Extension (KE) jet, low-frequency (>300 days) dipole (KED, hereafter) mode, and high-frequency (≤300 days) or mesoscale eddies in the upstream KE region using the data analysis and eddy-dipole mode interaction model. It is found that in a mean sense, the large KE jet meander (Fig. 1a) corresponds to a large-scale positive-over-negative dipole (KED^-) mode (Fig. 2a) in the upstream KE region with a strong EKE (Fig. 1e) and a double-branch jet structure with weak strength (Fig. 1c). In contrast, the small KE jet meander (Fig. 1b) corresponds to a large-scale negative-over-positive dipole (KED^+) mode (Fig. 2b) with a weak EKE (Fig. 1f) and a strong single-branch jet structure (Fig. 1d). We also examined the time evolution of the composite monthly mean SSH, zonal current velocity, and EKE anomalies of KED^- (KED^+) events. It is shown that when the KED^- mode intensifies (Fig. 3b), the KE jet is weakened and split to form a double-branch jet structure as a geostrophic balance (Fig. 4b) and the EKE is intensified in the upstream KE region (Fig. 5b). However, when the KED^+ mode strengthens (Fig. 3a), the KE jet is intensified to establish a single-branch jet structure (Fig. 4a) and is followed by the weakening of the EKE (Fig. 5a). Because the horizontal velocity ($\boldsymbol{V}$) and deformation field ($\boldsymbol{D}$) of the KED mode exhibits a decadal variation due to the PDO modulation, it is inevitable that the EKE shows a decadal change due to the roles of $-\boldsymbol{V}\cdot\nabla e$ and $\boldsymbol{E_m}\cdot\boldsymbol{D}$. Thus, the decadal variation of the EKE strength can be explained as the decadal change in the time-mean EKE associated with the frequency and phase of KED events (Fig. 11). For example, during a large KE jet meandering period, the mean EKE is strong because the number of KED^- modes is dominant. The reverse is true during a small KE jet meandering period.

The diagnostic results based on a new eddy-dipole mode interaction model presented here reveal that for the KED^-, the kinetic energy of mesoscale eddies grows by extracting energy from the KED^- shearing and stretching deformation fields and strengthens due to the reduced EKE advection because of a weakened KE jet as the KED^- mode intensifies (dashed line in Figs. 8 and 9b). However, for the KED^+, the mesoscale eddy energy weakens due to an enhanced EKE advection under an intensified KE jet and by losing energy to the KED^+ shearing and stretching deformation fields (solid line in Figs. 8 and 9a). This process results in a significant difference of the EKE strength in the upstream KE region between two phases of the KED mode. This can explain why there is a high (low) EKE level as observed during a large (small) KE meandering period, because the frequency of KED^- (KED^+) events is dominant.

The further calculation shows that while the EKE exhibits a maximum positive correlation of 0.74 with the PDO index at 3.4-year lag after the 11-month smoothing, the KED mode (KE jet strength) has a maximum negative correlation of −0.88 (−0.86) with the PDO index at the same time lag (Fig. 12). This suggests that the phase of the KED is mainly determined by the phase of the PDO. The decadal transition of the KED mode between its two phases leads to the decadal variability of the KE jet and EKE strengths in the upstream KE region.

On the other hand, it is worth pointing out that the eddy-dipole mode interaction model used here is barotropic and highly idealized. Nevertheless, as a first step such a treatment is acceptable if the KE current is assumed to be comprised of a upper active layer with an about 1000 m depth and a much deeper quiescent lower layer as done in Pierini (2006). This study can improve our better understanding of the dynamical mechanism of the decadal variability of the KE system. However, as noted by some studies, the baroclinic processes such as buoyancy forcing is also important for the variability of the KE system (Berloff et al. 2007a, b). Thus, an extended eddy-dipole mode interaction model is needed to understand the importance of baroclinic processes in the decadal EKE variability in that these processes have been neglected in our model. These problems deserve further investigation in the future.

Acknowledgments This work is supported by the National Key Program for Developing Basic Science of China (2013CB956203, 2011CB403500). The basic idea of this paper was proposed in 2013. The authors would like to thank Dr. Yu Zhang for her useful discussions on this paper and three anonymous reviewers for their useful suggestions which helped to improve this paper.

References

Berloff P, Hogg A, Dewar W (2007a) The turbulent oscillator: a mechanism of low-frequency variability of the wind-driven ocean gyres. J Phys Oceanogr 37:2363–2386

Berloff P, Kravtsov S, Dewar W, McWilliams J (2007b) Ocean eddy dynamics in a coupled ocean-atmosphere model. J Phys Oceanogr 37:1103–1121

Ceballos L, Di Lorenzo E, Hoyos CD, Schneider N, Taguchi B (2009) North Pacific gyre oscillation synchronizes climate variability in the eastern and western boundary current systems. J Clim 22:5163–5174

Chelton DB, Schlax MG, Samelson RM (2011) Global observations of nonlinear mesoscale eddies. Prog Oceanogr 91:167–216

Cushman-Roisin B (1986) Frontal geostrophic dynamics. J Phys Oceanogr 16:132–143

Deser C, Alexander MA, Timlin MS (1999) Evidence for a wind-driven intensification of the Kuroshio Current Extension from the 1970s to the 1980s. J Clim 12:1697–1706

Holloway G (2010) Eddy stress and shear in 2-D flow. J Turbulence 11:1–14

Holopainen E, Fortelius C (1987) High-frequency transient eddies and blocking. J Atmos Sci 44:1632–1645

Hoskins BJ, James IJ, White GJ (1983) The shape, propagation and mean-flow interaction of large-scale weather systems. J Atmos Sci 40:1595–1612

Jiang S, Jin F, Ghil M (1995) Multiple equilibria, periodic, and aperiodic solutions in a wind-driven, double-gyre, shallow-water model. J Phys Oceanogr 25:764–786

Kawai H 1972: Hydrography of the Kuroshio Extension. *Kuroshio*, 235–352.

Larichev, V. and G Reznik, 1976: Two-dimensional Rossby soliton: an exact solution. POLYMODE news, No. 19 (simultaneous Russian publication in Reports of U. S. S. R. Academy of Sciences, 1976, 231, No. 5)

Latif M, Barnett TP (1994) Causes of decadal climate variability over the North Pacific and North America. Science 266:634–637

Liu Z, Wu L (2004) Atmospheric response to North Pacific SST: the role of ocean-atmosphere coupling. J Clim 17:1859–1882

Luo D (2000) Planetary-scale baroclinic envelope Rossby solitons in a two-layer model and their interaction with synoptic-scale eddies. Dyn. Atmos Oceans 32:27–74

Luo D, Li J (2000) Barotropic interaction between planetary- and synoptic-scale waves during the life cycle of blockings. Adv Atmos Sci 17:649–670

Luo D, Cha J, Zhong L, Dai A (2014) A nonlinear multiscale interaction model for atmospheric blocking: the eddy-blocking matching mechanism. Quart J Roy Meteor Soc 140:1785–1808. doi:10.1002/qj.2337

Luo D, Zhong L, Franzke C (2015) Inverse energy cascades in an eddy-induced NAO-type flow: scale interaction mechanism. J Atmos Sci 72:3417–3448

Mak M, Cai M (1989) Local barotropic instability. J Atmos Sci 46:3289–3311

McCalpin JD, Haidvogel DB (1996) Phenomenology of the low-frequency variability in a reduced-gravity, quasi-geostrophic double-gyre model. J Phys Oceanogr 26:739–752

Mizuno K, White WB (1983) Annual and interannual variability in the Kuroshio current system. J Phys Oceanogr 13:1847–1867

Nonaka M, Nakamura H, Tanimoto Y, Kagimoto T, Dasaki H (2006) Decadal variability in the Kuroshio–Oyashio Extension simulated in an eddy-resolving OGCM. J Clim 19:1970–1989

Pierini S (2006) A Kuroshio Extension system model study: decadal chaotic self-sustained oscillations. J Phys Oceanogr 36:1605–1625

Pierini S (2014) Kuroshio Extension bimodality and the North Pacific Oscillation: a case of intrinsic variability paced by external forcing. J Clim 27:448–454

Pierini S, Dijkstra H, Riccio A (2009) A nonlinear theory of the Kuroshio Extension bimodality. J Phys Oceanogr 39:2212–2229

Qiu B, Chen S (2005) Variability of the Kuroshio Extension jet, recirculation gyre, and mesoscale eddies on decadal time scales. J Phys Oceanogr 35:2090–2103

Qiu B, Chen S (2010) Eddy-mean flow interaction in the decadally modulating Kuroshio Extension system. Deep-Sea Res II Top Stud Oceanogr 57:1098–1110

Sasaki Y, Minobe S, Schneider N (2013) Decadal response of the Kuroshio Extension jet to Rossby waves: observation and thin-jet theory. J Phys Oceanogr 43:442–456

Seager R, Kushnir Y, Naik NH, Caneand MA, Miller J (2001) Wind-driven shifts in the latitude of the Kuroshio - Oyashio Extension and generation of SST anomalies on decadal timescales. J Clim 14:4249–4265

Serazin G, Penduff T, Gregorio S, Barnier B, Molines J, Terray L (2015) Intrinsic variability of sea-level from global 1/12 ocean simulations: spatio-temporal scales. J Clim 28:4279–4292

Stern ME (1975) Minimal properties of planetary eddies. J Mar Res 33:1–13

Taguchi BS-P, Xie N, Schneider M, Nonaka HS, Sasai Y (2007) Decadal variability of the Kuroshio Extension: observations and an eddy-resolving model hindcast. J Clim 20:2357–2377

Waseda T, Mitsudera H, Taguchi B, Yoshikawa Y (2002) On the eddy-Kuroshio interaction: evolution of the mesoscale eddy. J. Geophys. Res. Oceans 107(C8):1–19. doi:10.1029/2000JC000756

Waterman S, Hogg NG, Jayne SR (2011) Eddy-mean flow interaction in the Kuroshio Extension region. J Phys Oceanogr 41:1182–1208

Wyrtki K (1975) Fluctuations of the dynamic topography in the Pacific Ocean. J Phys Oceanogr 5:450–459